Irina Gruber, Lisa Bensch, Thomas J. J. Müller, Christoph Janiak and Birger Dittrich*

Studying the hydrogen atom position in the strong-short intermolecular hydrogen bond of pure and 5-substituted 9-hydroxyphenalenones by invariom refinement and ONIOM cluster computations

https://doi.org/10.1515/zkri-2020-0022
Received March 2, 2020; accepted May 4, 2020; published online June 3, 2020

Abstract: The solid-state structures of three H-bonded enol forms of 5-substituted 9-hydroxyphenalenones were investigated to accurately determine the H atom positions of the intramolecular hydrogen bond. For this purpose, single-crystal X-ray diffraction (SC-XRD) data were evaluated by invariom-model refinement. In addition, QM/MM computations of central molecules in their crystal environment show that results of an earlier standard independent atom model refinement, which pointed to the presence of a resonance-assisted hydrogen bond in unsubstituted 9-hydroxyphenalone, are misleading: in all our three and the earlier solid-state structures the lowest energy form is that of an asymmetric hydrogen bond (C_S form). Apparent differences of results from SC-XRD and other analytical methods are explained.

Keywords: intramolecular hydrogen bond; ONIOM QM/MM computations; single-crystal X-ray diffraction; 5-substituted 9-hydroxyphenalenone derivatives; invariom refinement.

***Corresponding author: Birger Dittrich**, Institut für Anorganische Chemie und Strukturchemie II, Heinrich-Heine-Universität Düsseldorf, Universitätsstraße 1, 40225 Düsseldorf, Germany, E-mail: dittrich@hhu.de. https://orcid.org/0000-0002-4306-5918
Irina Gruber and Christoph Janiak: Institut für Anorganische Chemie und Strukturchemie, Heinrich-Heine-Universität Düsseldorf, Universitätsstraße 1, 40225 Düsseldorf, Germany, E-mail: irina.gruber@uni-duesseldorf.de (I. Gruber), janiak@uni-duesseldorf.de (C. Janiak). https://orcid.org/0000-0002-6288-9605 (C. Janiak)
Lisa Bensch and Thomas J. J. Müller: Institut für Organische Chemie und Makromolekulare Chemie, Heinrich-Heine-Universität Düsseldorf, Universitätsstraße 1, 40225 Düsseldorf, Germany, E-mail: lisa.bensch@uni-duesseldorf.de (L. Bensch), ThomasJJ.Mueller@hhu.de (T.J.J. Müller). https://orcid.org/0000-0001-9809-724X (T.J.J. Müller)

1 Introduction

The hydrogen bond is unique due to its adaptable combination of electrostatics and covalency. Moreover, it is important for numerous processes in chemistry and biochemistry [1–4]. A strong or classic hydrogen bond occurs when there is an interaction between an electron-rich atom (A), and a sufficiently positively polarized H atom, which is part of a covalent bond with an electronegative atom (D). The D–H···A hydrogen bond can appear either between different molecules (intermolecular) or within the same molecule (intramolecular). In both cases, the D–H bond distance is to some extent elongated when compared to equivalent distances where the acceptor atom (A) is absent. A special kind of hydrogen bond has been reported where the proton is shared equally between the atoms D and A (D···H···A). Here short H···A distances lead to an effective coupling between two covalent, and one ionic valence bond structures in a low barrier hydrogen bond (LBHB, see Figure 1) [5–8].

Four characteristics for such LBHBs have been defined [9, 10]: firstly, the D···H and H···A distances between the atoms in D···H···A are longer compared with normal D–H and H–A covalent bonds and secondly, the D···H···A bonds are based on two energetically equivalent atomic arrangements, where each can be formally described by different mesomeric Lewis structures. Thirdly, the fast equilibrium through the D···H···A transition state leads to an energetic stabilization, which grants the fourth feature, namely that also the D···A distance is shorter than in a normal hydrogen bond. Enolized diketones, which are stabilized by intramolecular OHO hydrogen bonds, are usually thought of as being centered, linear hydrogen bonds that are involved in the delocalized π-system to give "aromatic" systems [11]. Such special or near-symmetric hydrogen bonds are often formed between charged moieties. For O–H···O systems these special hydrogen bonds can be frequently found when O···O distances are short (below 2.5 Å). For cases where a short-strong hydrogen bond exists, Gilli et al. introduced the term resonance-assisted hydrogen bond (RAHB) as a

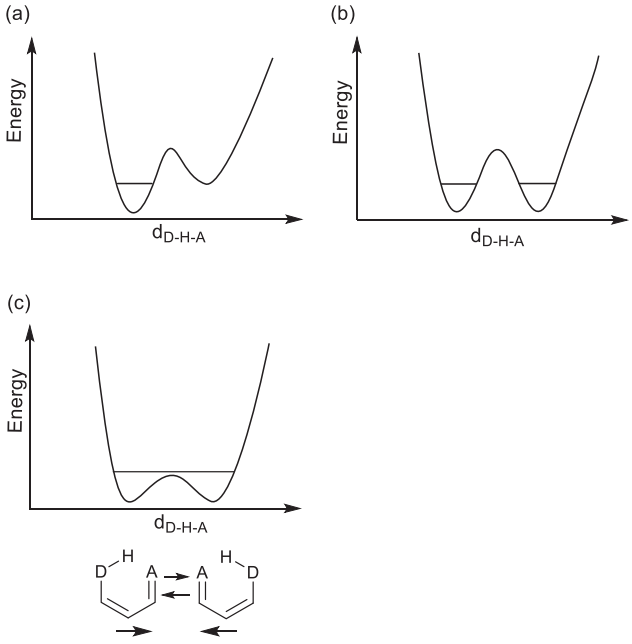

Figure 1: Schematic potential–energy curves for hydrogen bonds (D–H···A). Asymmetric double-well potential (a), symmetric double-well potential (b) and low barrier hydrogen bond LBHB (c). In the LBHB case two proton normal modes D–H···A and A···H–D are shown. The thick arrows indicate the transverse dipole moment which inverts with tautomerization.

particular case of an intramolecular hydrogen bond in 1989. RAHBs are supported by a conjugated π-electron system (see Figure 2) where six-, eight-, or ten-membered neutral rings are formed [12–14].

The unsubstituted enolized diketone 9-hydroxyphenalen-1-one (9-HP) can exist in C_{2v} or C_S form with a six-membered H-bonded ring. In solution, as shown by ^{1}H and ^{13}C NMR studies [15], 9-HP appears to have C_{2v} symmetry down to a temperature of 130 K. The higher symmetry could of course be due to rapid interconversion between its two C_S forms. An IR spectroscopic investigation of both solution and solid state found no absorption for the O–H stretching band due to the presence of very strong intramolecular hydrogen bonding

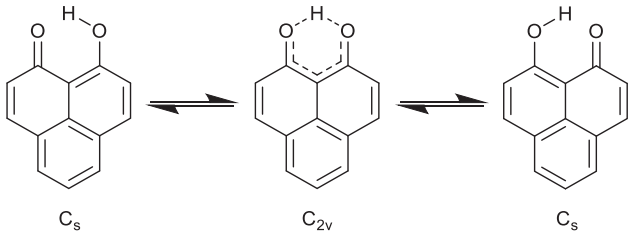

Figure 2: Interconversion between two equivalent minimum energy (C_S) structures with asymmetric hydrogen bridges in 9-hydroxyphenalen-1-one as an example of an enolized diketone or hydroxyl ketone. The interconversion occurs through a symmetric (C_{2v}) (transition-state) intermediate.

with the carbonyl oxygen [16]. Studies using single-crystal X-ray diffraction (SC-XRD) have shown that 9-HP possesses a short O–O distance (<2.5 Å) [17], and that there is a phase transition between a low-temperature C_S form with four molecules in the asymmetric unit (Z' = 4, CSD refcode HXPHOL11, 215 K), and a room-temperature C_{2v} structure with Z' = 2 where one molecule is disordered, whose H-atoms were omitted in the deposition refcode HXPHOL [18].

The combined use of ^{13}C and ^{2}H spin-lattice relaxation times provides a convenient means of determining quadrupole coupling constants of intramolecular bridging deuterons in planar molecules in the liquid phase. In systems of the type D–^{2}H···A (^{2}H = deuteron), the strength of the "hydrogen bond" is related to the position of the deuteron relative to D and A, which, in turn, controls the magnitude of the quadrupole coupling constant. Thus, values of this coupling constant provide a qualitative criterion of the strengths of hydrogen bonds in series in which D and A are held constant [19]. The D···H···A linear motion may strongly couple with the other two-proton normal modes (D–H···A and A···H–D), producing a three-dimensional oscillation. There might also be strong anharmonic coupling between D···H···A and the oxygen-atom normal modes due to the fact that the proton at the top of the barrier undergoes a subtle balance of forces [20]. For the intramolecular proton exchange in 9-HP, tunneling can be calculated from the energy difference between the gerade–ungerade pair. Such a calculation is based on the proton, which will spend equal time in each well, and tunneling will depend on the frequency with which the proton oscillates between the wells [21]. Gilli et al. differentiated three ways for making the two resonant forms of intramolecular hydrogen bonds equivalent (see Figure 3) [22] and further categorized hydrogen bonds as:

- resonance-assisted hydrogen bonds (RAHBs, here the two oxygen atoms are interconnected by a system of π-conjugated double bonds (–O–H···O=),
- charged assisted hydrogen bonds (CAHB, divided into negative (–O–H···O$^-$–) and positive (=O···H$^+$···O=), also known as (–/+)CAHB), and
- low barrier hydrogen bonds (LBHB) [23].

According to Emsley's empirical studies, the delocalization of the π-conjugated system becomes greater in case the hydroxyl-ketone unit forms either intra-molecular, or infinite-chain intermolecular hydrogen bonds [11].

9-Hydroxyphenalenone and its derivatives are suitable examples for investigating such strong hydrogen bonds of keto–enols. The molecule contains a hydroxyl ketone unit [24] and is an electron acceptor, known for its ability to react as a radical anion [25, 26], but is also known for forming metal complexes [27–30]. It was first synthesized by Koelsch in 1941

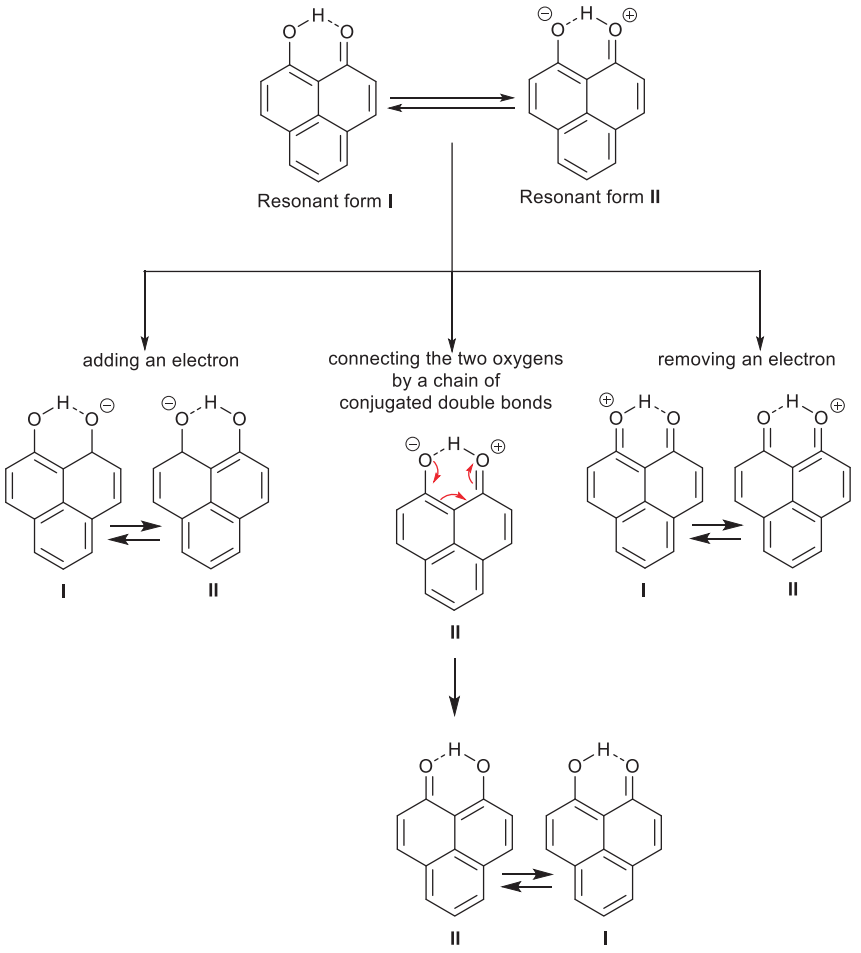

Figure 3: Two resonant forms **I** and **II** and three possible ways to interconvert them.

[31]. Derivatives are used for many different applications [25], in particular as ligand in transition metal catalysts [32] and as neutral radical conductors [33]. The functionalization in the 5-positions of 9-HP has remained rather rare [27, 34], but was systematically investigated by DFT computations by Bensch et al., who considered electronic and photophysical properties [35], and also highlighted that conjugated 5-substituted 9-HP systems are synthetically accessible without the necessity of protecting the hydroxyl group due to the strong intramolecular hydrogen bond.

For 9-HP, the high temperature structure [18] indicates that a symmetric intramolecular hydrogen bond is present (symmetric C_{2v} form, Figure 2). Since an O–H stretching band could not be found in the IR spectrum due to the presence of a very strong intramolecular hydrogen bonding with the carbonyl oxygen [16], and since 9-HP exhibits ^{1}H and ^{13}C NMR spectra which are consistent with either C_{2v} symmetry or with existence of rapidly equilibrating C_S tautomers [36], the question arises how the results from different spectroscopic techniques and SC-XRD can be joined, understood and consistently united. Variable-temperature NMR studies on 9-HP and hydrogenated malonaldehyde, the latter also in its deuterated form, also support occurrence of fast interconversion between asymmetrically hydrogen bonded structures of such bistable molecules, resulting in rapid prototropy between two equivalent tautomers (see Figure 3) [15, 36]. X-ray photoelectron spectroscopy (XPS) spectra showed that the H atom remains localized on one oxygen atom for at least a few O–H vibrational periods [16]. These results have been validated by deuteron quadrupole coupling constants which were shown to be linearly related to the squares of stretching frequencies for the corresponding X–H bonds and suggest that 9-HP involves hydrogen bonds with double-well potentials. Vibronically resolved fluorescence and fluorescence excitation spectra of 9-HP show strong spectral changes when the phenolic proton is deuterated, implying that the proton motion is coupled to a rearrangement of the oxygen-carbon molecular framework, and double-minimum potential energy curve shapes were calculated for both ground and electronically excited state [20]. Moreover, it has been calculated that the proton experiences a tunneling effect and therefore a double minimum potential, implying structural alterations regarding the equilibrium configuration and the transition state [37]. Ab initio SCF calculations on 9-HP supported the existence of two equivalent minimum-energy structures with an

asymmetric hydrogen bridge (C_S, Figure 2). According to these computations the interconversion between the two minima occurs through a symmetric (C_{2v}) intermediate which is 5.20 kcal/mol above the minimum-energy C_S structures [38]. How do the results from SC-XRD fit into this picture?

9-HP contains a strong intramolecular hydrogen bond forming a fourth six-membered ring. While all spectroscopic methods and gas-phase computations agree on the hydrogen bonds in 9-HP having double-well potentials and two discrete minima, the high-temperature form of the crystal shows a symmetric intramolecular hydrogen bond [18, 39]. Hence, we set out to investigate three recently synthesized 9-HP derivatives with substituents in the 5-position (summarized in Table 1) by SC-XRD, and complemented the experimental studies by QM/MM cluster computations which take into account the influence of the solid state. These computations were also performed on 9-HP. SC-XRD studies made use of invariom [40] aspherical scattering factors that permit obtaining more precise especial results than IAM refinement [41]. Using invariom-model refinement [42], which relies on the Stewart–Hansen–Coppens multipole model [43, 44] we thus aim for an accurate determination of the position of the hydrogen atoms participating in the strong hydrogen bond, and will find an encompassing explanation for the apparently contradictory spectroscopic and crystallographic results.

2 Experimental

2.1 Materials

Single crystals of 9-hydroxy-5-(4-methoxyphenyl)-1*H*-phenalen-1-one (**I**), 9-hydroxy-5-(1-methyl-1H-pyrazol-4-yl)-1H-phenalen-1-one (**II**) and 5-[4-(9H-carbazol-9-yl) benzyl]-9-hydroxy-1H-phenalen-1-one (**III**) were prepared as described elsewhere [33, 45].

2.2 SC-XRD data collection

All single-crystals were carefully selected under a polarizing microscope and mounted in oil on a loop. Data for initial structure solution were collected using ω-scans on a Bruker Kappa APEX2 CCD Duo diffractometer with microfocus sealed tube, using Cu–Kα radiation (λ = 1.54178 Å) for **I**, and Mo–Kα radiation (λ = 0.71073 Å) for **II** and **III**. In order to have diffraction data of similar quality and resolution for all three compounds, X-ray diffraction data for **I**–**III** were then re-measured at a temperature of 100 ± 2 K at the SLS synchrotron beamline X10SA with a wavelength of 0.6358 Å using 360 degree Φ scans with a DECTRIS Pilatus 6M detector. Cell refinement, and data reduction employed the XDS program [46]. Preliminary refinement was done by full-matrix least squares on F^2 using SHELXL-2016 [47]. Empirical (multi-scan) absorption correction was achieved with SADABS [48]. Crystal structure and refinement data are presented in Table 2.

2.3 Least-squares refinement and electron density modeling using invariom

All non-hydrogen positions for **I**–**III** were refined with anisotropic displacement parameters. For later comparison with the invariom model [40] SHELXL independent atom model (IAM) refinement was repeated with the XD program suite [50]. In addition, the IAM result provided input for subsequent invariom [42] least-squares refinement with Stewart–Hansen–Coppens [43, 44] aspherical scattering factors predicted by DFT computations. IAM and invariom refinement in XD were carried out using the same X-ray diffraction intensities (merged for **I** and **II**, but not **III**), weighting schemes and cutoff settings. Since the scattering factors for some of the more unusual model compounds were not initially present in the invariom database, several missing model compounds were added. A Holstein assignment diagram that contains the central molecule, the model compounds with their SMILES [51] code and the respective IUPAC name are shown exemplarily for molecule **I**. The other Holstein plots can be found in the supplementary information. For all geometry optimizations underlying the database, the same M06/def2TZVP DFT method/basis set combination was chosen. Computations using the program GAUSSIAN09 [52] and subsequent Fourier transform with the TONTO program [53] permitted to generate static structure factors from the wavefunctions obtained; each model compound was then fitted with a multipole model; the

Table 1: 5-Substituted 9-hydroxyphenalenones studied here by SCXRD.

Parent molecule	R	Code	Name
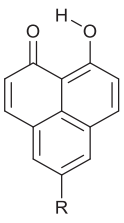	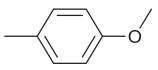	I	9-Hydroxy-5-(4-methoxyphenyl)-1H-phenalen-1-one
	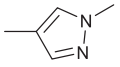	II	9-Hydroxy-5-(1-methyl-1H-pyrazol-4-yl)-1H-phenalen-1-one
	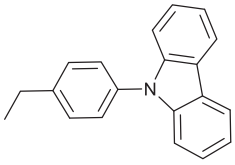	III	5-[4-(9H-Carbazol-9-yl)benzyl]-9-hydroxy-1H-phenalen-1-one

Table 2: Crystal structure and refinement data for **I**–**III**, the three 5-substituted 9-HP samples used in this study.

Crystal data	**I**	**II**	**III**
Chemical formula	$C_{20}H_{14}O_3$	$C_{17}H_{12}N_2O_2$	$C_{32}H_{21}NO_2$
M_r	302.31	276.29	451.50
Crystal system, space group	Monoclinic, $P2_1/c$	Orthorhombic, $Pna2_1$	Orthorhombic, $Fdd2$
Temperature (K)	100	100	100
a, b, c (Å)	3.803 (1), 14.230 (4), 26.66 (2)	20.560 (5), 13.587 (8), 4.689 (1)	13.766 (5), 62.85 (3), 10.3805 (15)
β (°)	92.512 (13)	90	90
V (Å^3)	1441.3 (12)	1309.9 (9)	8981 (5)
Z	4	4	16
Radiation type	Monochromatised beam (SLS synchrotron), λ = 0.6358 Å		
μ (mm^{-1})	0.07	0.07	0.07
Crystal size (mm)	0.25 × 0.09 × 0.09	0.09 × 0.05 × 0.05	0.11 × 0.05 × 0.05
Data collection and Refinement			
Diffractometer	Diffractometer at beamline X10SA (SLS)		
Absorption correction	Empirical (using intensity measurements) *SADABS* version 2016/2, multi-scan. (G. M. Sheldrick, 2016)		
T_{min}, T_{max}	0.630, 0.745	0.712, 0.745	0.673, 0.746
No. of measured, independent and observed ($I > 2\sigma(I)$) reflections	32598, 2557, 2467	35995, 2990, 2982	88527, 8014, 7892
R_{int}	0.061	0.040	0.053
$(\sin\theta/\lambda)_{max}$ (Å^{-1})	0.599	0.649	0.759
$R[F^2 > 2\sigma(F^2)]$, $wR(F^2)$, S	0.05, 0.157, 4.23	0.03, 0.095, 4.81	0.037, 0.093, 3.45
No. of reflections	2467 (96.4% compl.)	2982 (99.7% compl.)	7892 (98.4% compl.)
No. of parameters	264	237	399
$\Delta\rho_{max}$, $\Delta\rho_{min}$ (e Å^{-3})	0.38, −0.34	0.23, −0.19	0.79, −0.29
Absolute structure	–	–	Flack x determined using 3,670 quotients [(I+)−(I−)]/[(I+)+(I−)] [49]
Absolute structure parameter	–	–	0.00 (15)

multipole parameters with their local pseudoatom coordinate system then constitute a scattering factor database entry. The program XDLSM [49] was employed for both the aspherical-atom refinements on the 'simulated' theoretical data, as well as the later refinements with the experimentally measured data. Concerning the treatment of hydrogen atoms in the experimental XDLSM refinement, riding hydrogen atom positions from the IAM were initially used as starting point. The X–H bonds were then elongated to the M06/def2TZVP optimized result, with freely adjusted isotropic displacement parameters. Finally, for finding the hydrogen atom of the strong O–H···O hydrogen bond, ultimately all hydrogen atom positions were allowed to adjust in addition to their isotropic displacement parameters. XD input files were generated with the preprocessor program Invariomtool [54]. Structural data for this paper have been deposited with the Cambridge Crystallographic Data Center (CCDC-numbers 1831535 (**I**), 1831536 (**II**), 1831537 (**III**)). These data can be obtained free of charge via www.ccdc.cam.ac.uk/data_request/cif.

3 Results and discussion

The Holstein plot in Figure 4 and Supplementary Figure S1 shows the fragmentation of the molecules into invariom and the model compounds that were necessary to generate them. The molecular electron density can then be reconstructed from these fragments. To obtain the Holstein plot and invariom name, the local connectivity of an atom with the respective bond-distinguishing parameter, as provided by the preprocessor program INVARIOMTOOL [53], was evaluated. This invariom string was then re-interpreted to give the required model compounds. To facilitate the reproduction of this work, the SMILES string is also provided.

It would have been easier to simply calculate the molecular electron density once, if the purpose had been to model the electron density of only one of the molecules. However, for a series of molecules the model compounds are the same, apart from a few additional ones in each case. Invariom are available from a database. Since computations of model compounds for invariom present in the database do not need to be repeated, computation time is saved overall. At the same time the coverage of existing model compounds is continuously expanded, directly covering even more compounds.

Figure 5 shows the result of including aspherical electron density in the scattering factor model for the three molecules in form of a deformation electron density plot. As has been shown earlier, e.g., in [55], the residual electron density is usually reduced after invariom refinement, unless there is disorder or there are other crystallographically important effects that can be overlooked more easily in IAM refinement. Residual electron density due to covalent bonding is absent and faithfully taken into account in all three invariom refinements. Isotropic displacement parameters for hydrogen atoms are also visualized in Figure 5, and from their size one can see that the hydrogen atoms participating in the strong O–H···O hydrogen bond in **I** and **II** have a larger vibrational amplitude than the other hydrogen atoms, similar to methyl hydrogens prone to rotational disorder. While there is residual electron density in **III** behind and in between the O–H···O oxygen atom of 0.15 e, the hydrogen atom can be located rather precisely in **I**, **II**, and **III**. The highest residual electron density peak in **III** is higher in invariom than in IAM refinement, but close to C14, which links the two extended ring systems, i.e., far away from the hydrogen atom of interest.

From all three aspherical-atom structure analyses of **I**, **II** and **III** it can be seen that the hydrogen atoms of interest are localized at only one of the two possible oxygen atoms. While the situation still corresponds to an LBHB in these substituted 9-HP derivatives, the hydrogen atoms are located on average in only one of the two possible energy minima throughout the whole crystal. Further details on the exact hydrogen bonding situation are provided in Table 3.

4 ONIOM computations

In light of the challenge to understand the apparently different analytical results of SC-XRD, IR, NMR and XPS, it is desirable to have a complementary method that probes the solid state to support our interpretation. Therefore, two layer QM/MM ONIOM [57] computations were performed on the asymmetric unit molecules (all structures have $Z' = 1$) in the surrounding of their nearest neighbor molecules that were generated from space-group symmetry using the program BAERLAUCH [58]. Before we discuss the results of a geometry optimization of the central molecule in the cluster, we start discussing the role of space-group symmetry, since this aspect can be relevant for the formation of symmetric or unsymmetrical hydrogen bonding (be it static in time or dynamic).

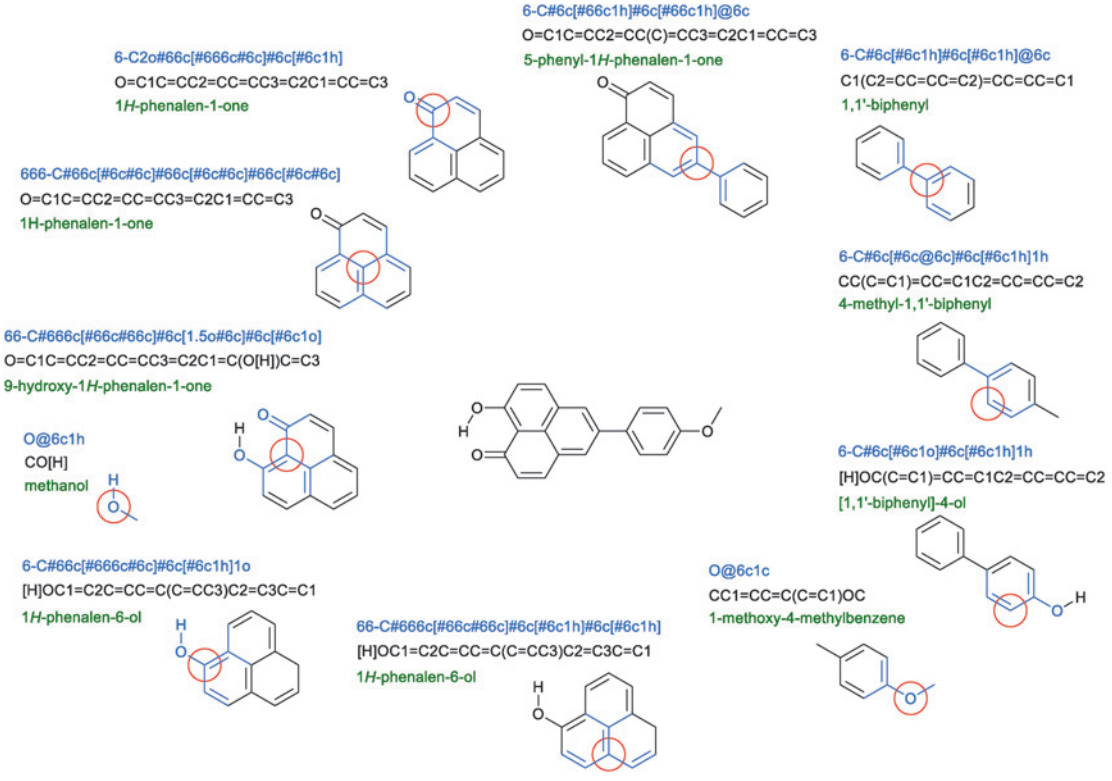

Figure 4: A representation of model compounds used to reproduce aspherical electron densities for 9-hydroxy-5-(4-methoxyphenyl)-1H-phenalen-1-one. Blue color was used for the invariom name of an atom of interest. SMILES and IUPAC names are also provided. The latter describe whole molecules, while the invariom notation defines the local chemical environment of an atom.

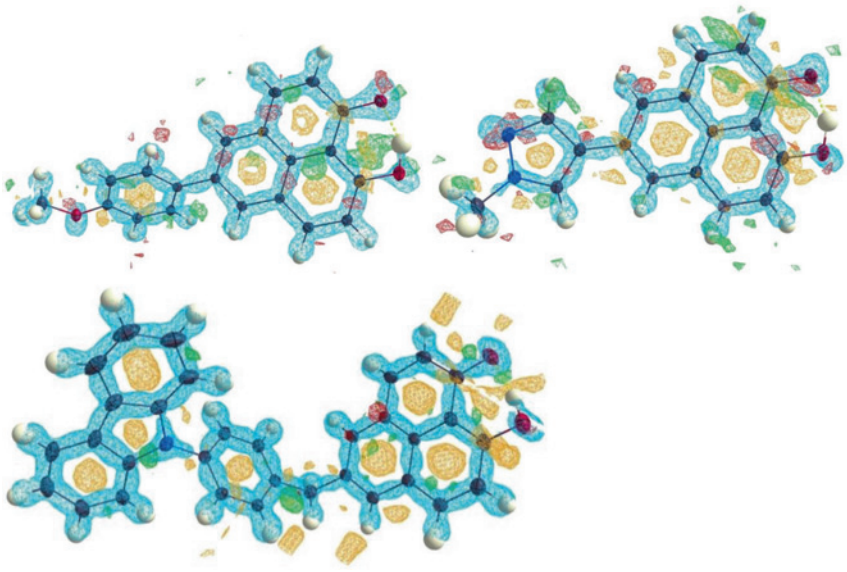

Figure 5: A combination of an ORTEP plot of anisotropic/isotropic displacement parameters (50% probability), the deformation electron density and the remaining residual electron density shown for all three molecules. For **I** (top left) only residuals above 0.2 e are shown, for **II** (top right) this threshold value was set to 0.1 e and for **III** (below) it was 0.15 e. Figures were generated with MOLECOOLQT [56].

Table 3: Hydrogen-bonding scheme (Å, °) in the three derivatives of 9-HP.

O1–H1···O2	I	II	III
D–H	0.99 (3)	1.04 (2)	0.89 (2)
H···A	1.62 (3)	1.56 (2)	1.640 (19)
D···A	2.529 (2)	2.520 (2)	2.5127 (18)
D–H···A	151 (2)	152 (2)	166.7 (18)

Compound **I** fulfills the symmetry of the common monoclinic space group $P2_1/c$ in the solid, and one can see from the illustration (Figure 6) of neighboring molecule in the cluster that the combination of a 2_1 screw axis and a *c*-glide plane leads to an inversion center, so that for all O–H···O moieties there is an O···H–O pendant due to symmetry. Therefore, the in-plane dipole-moment contributions of the intramolecular hydrogen bonds will cancel out in the crystal. Due to the glide plane the situation is analogous in **III**, space group *Fdd*2, where however no inversion center is present (the only structure for which a Flack-parameter is reported). In **II**, which crystallizes in the non-centrosymmetric space group $Pna2_1$, there is also one site for the hydrogen atom only, and molecular in-plane contributions cancel due to π-stacking. We therefore think that the electric field of the crystals does not play the decisive role in the hydrogen position in the O–H···O hydrogen bond. We note that the dipole moment contributions also cancel when there is a dynamic exchange in between them.

This is supported by the result of the ONIOM B3LYP/6-31G(d,p): UFF geometry optimization of the central molecules in their respective clusters as generated from the invariom refined structures. Figure 6 shows exemplarily the cluster of **I** with 15 molecules, emphasizing the central molecule of the asymmetric unit. The number of molecules (**II**: 17 molecules, **III**: 16 molecules) depends on space-group symmetry and crystal packing. A molecule was included in the clusters when a surrounding atom in a neighboring molecule was within 3.75 Å of any of the atoms in the asymmetric unit.

Bond distances from these computations corresponding to those given for the experimental structures from invariom refinement are given in Table 4 alongside the experimental data. These data show that the global minimum of the DFT optimized asymmetric unit molecule in a cluster of MK point charges [59], with the molecular surrounding subjected to a UFF force field treatment [60], fully confirm the hydrogen positions of the structures **I**, **II**, and **III**. It inspires confidence how well experiment and theory agree, not only among themselves, but also for all three compounds. The only outlier is the experimentally short O1-H1 bond in **III**, which also affects the bond angle δ. Otherwise there is often quantitative agreement within 3 σ.

5 Discussion: does the LBHB lead to a shared H position in the middle of the two oxygen atoms?

After re-refining three crystal structures of 9-HP derivatives with aspherical scattering factors of the invariom database we find no convincing evidence for a symmetric "resonance assisted" hydrogen bond in these molecules, and a symmetric hydrogen bond can be clearly ruled out at the measurement temperature of 100 K. Although in **III** residual electron density is in the order of magnitude of the

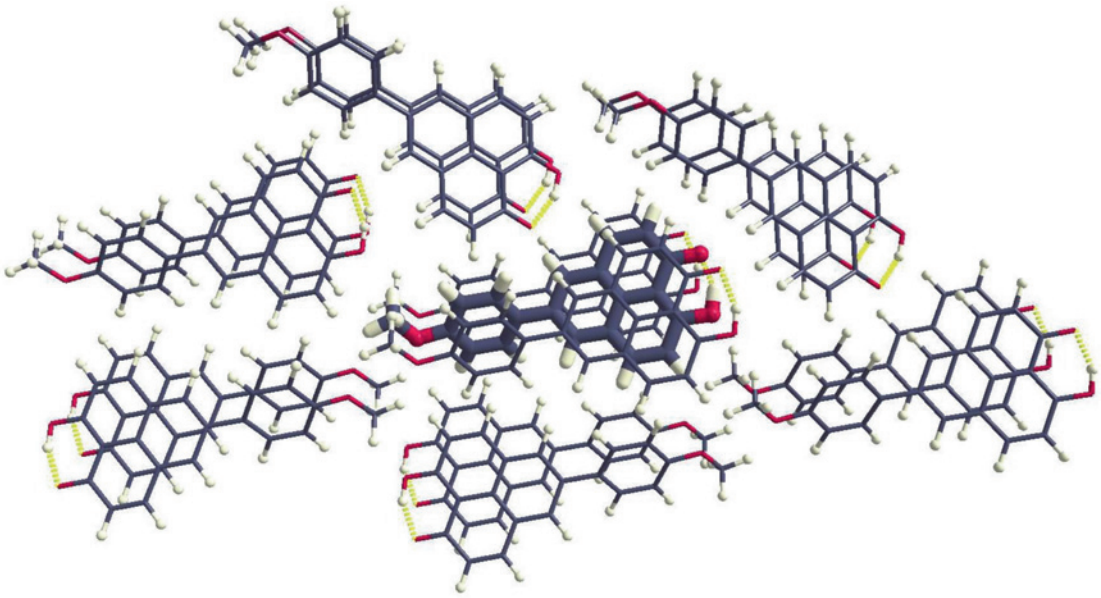

Figure 6: Depiction of the cluster used in the ONIOM B3LYP/6-31G(d,p):UFF computation of **I**. The central molecule is emphasized. The invariom result, including the hydrogen atom positions after invariom refinement, was used to generate the input.

signal of covalent bonding, and these signals remain after invariom refinement, residual electron density features are far away from the hydrogen atom in question and do not compromise this result. The experimental results are also in nice agreement with two layer ONIOM computations, and both methods provide a consistent answer. In these computations the coordinates of the experimental crystal structure provide the cluster molecules after applying symmetry, and only the central molecule is optimized. The cluster environment is representative of the crystal field, and the method permits to identify the hydrogen-atom position corresponding to the solid-state energy minimum.

So how do these results with local C_S symmetry fit together with the original C_{2v} symmetric high-temperature structure determination for 9-HP [18]? The results for **I**, **II**, and **III** apparently agree only with the low-temperature form of 9-HP (refcode HXPHOL11), where again located hydrogen atoms were found by SC-XRD, but not with the room-temperature structure. Therefore, we have also performed ONIOM computations analogous to those described earlier for **I**, **II**, and **III** on the 9-HP room temperature structure using the deposited refcode HXPHOL as input. A difference was that we had to add several missing hydrogen atoms, so we added a pre-optimization step of the central molecule in the cluster with the XTB program [61]. Since in space group is $P2_1/c$ there were two possible input structures for the missing hydrogen atom of interest, both of them were computed. Like for **I**, **II**, and **III** both these structures have located hydrogen positions after optimization. Their energy is similar, the relative energy difference for the central molecule in the cluster is 4.1 kcal/mol, which is probably within the accuracy of the computational method. The temperature-dependent disorder (and the phase transition) in 9-HP commences when the energy difference between the lower energy and the higher energy structure can be overcome. H atoms are thus *not* shared between the two oxygen atoms, and are alternating between molecules related by mirror plus glide plane according to space-group symmetry, again canceling the local dipole moments. We conclude that the room-temperature structure of 9-HP is, analogous to the NMR results, a disordered overlay of the two possible individual structures. We have to remind ourselves that in SC-XRD we obtain positions from a time and space average of a large number of unit cells. When for 9-HP the thermal motion of the atoms increases, the average of the individual structures starts to agree with higher space-group symmetry, which also leads to an apparently shared hydrogen atom between the oxygen atoms. Other factors are the resolution of the experiment, which is necessarily limited, and tunneling. However, individual contributor structures still have localized hydrogen atoms. Even measuring diffraction data to higher resolution would not change this apparent C_{2v} symmetry, whereas smaller thermal motion (lowering the temperature) leads to the phase transition in 9-HP. Hydrogen atoms in individual molecules remain located at one oxygen atom in both contributing structures for time periods longer than can be probed by an SC-XRD measurement,

Table 4: Selected distances (Å) for the three 5-substituted 9-HP samples used in this study.[a]

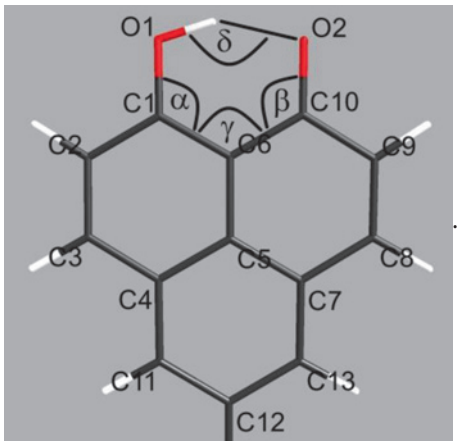

	I-XRD	I-ONIOM	II-XRD	II-ONIOM	III-XRD	III-ONIOM
O1–C1	1.333 (2)	1.3265	1.3368 (16)	1.3255	1.3195 (18)	1.3262
O2–C10	1.284 (2)	1.2603	1.2765 (16)	1.2595	1.2660 (18)	1.2580
O1–H1	0.99 (3)	1.0202	1.04 (2)	1.0243	0.888 (19)	1.0142
C1–C6	1.424 (2)	1.4115	1.4192 (17)	1.4094	1.4117 (15)	1.4085
C1–C2	1.438 (2)	1.4222	1.4310 (17)	1.4229	1.4196 (19)	1.4212
C2–C3	1.380 (2)	1.3712	1.3840 (18)	1.3721	1.3685 (19)	1.3716
C3–C4	1.434 (2)	1.4214	1.4410 (17)	1.4277	1.4298 (14)	1.4239
C4–C11	1.419 (2)	1.4087	1.4200 (17)	1.4083	1.4125 (18)	1.4132
C4–C5	1.431 (2)	1.4201	1.4270 (19)	1.4238	1.4098 (18)	1.4207
C5–C6	1.429 (2)	1.4166	1.4298 (18)	1.4149	1.4189 (18)	1.4163
C5–C7	1.431 (2)	1.4237	1.4316 (17)	1.4232	1.4169 (13)	1.4207
C6–C10	1.456 (2)	1.4558	1.4544 (19)	1.4555	1.4510 (19)	1.4595
C7–C13	1.408 (2)	1.3929	1.4016 (17)	1.3907	1.3921 (18)	1.3896
C7–C8	1.455 (2)	1.4444	1.4509 (19)	1.4446	1.4446 (19)	1.4399
C8–C9	1.366 (2)	1.3592	1.3656 (17)	1.3590	1.3558 (19)	1.3555
C9–C10	1.463 (2)	1.4557	1.4649 (17)	1.4534	1.4462 (16)	1.4525
α	120.78 (13)	121.19	120.66 (9)	120.89	120.91 (12)	121.07
β	120.72 (13)	120.70	120.77 (10)	120.55	121.02 (10)	121.21
γ	120.00 (13)	119.35	119.93 (9)	119.30	119.71 (11)	119.77
δ	151 (2)	152.47	152 (2)	153.35	166.7 (18)	152.33

[a]XRD = X-ray diffraction and ONIOM = two layer ONIOM computation.

despite but still in agreement with the higher symmetry at room temperature.

6 Conclusions

While room-temperature SC-XRD using the IAM for 9-HP apparently disagreed initially with other spectroscopic results, cluster computations in addition to earlier low-temperature SC-XRD data collection and analysis falsify the presence of a C_{2v} symmetric RAHB in 9-HP. These results are fully supported by IAM as well as more precise invariom refinements of three more substituted 9-HP derivatives reported here. ONIOM cluster computations complement and nicely confirm the analysis. Residual electron density obtained after invariom refinement was shown to be a useful validation tool in this context – recent technical progress in evaluating single crystal X-ray diffraction data does provide an unambiguous result in full agreement with other spectroscopic results as well as DFT computations on clusters of molecules that represent the solid state.

Acknowledgments: We thank the DFG, project DI 921/6-1, for financial support.

Author contribution: All the authors have accepted responsibility for the entire content of this submitted manuscript and approved submission.
Research funding: B.D. acknowledges funding from the Deutsche Forschungsgemeinschaft DFG, project DI 921/6-1.
Conflict of interest statement: The authors declare no conflicts of interest regarding this article.

References

1. Jeffrey G. A. *An Introduction to Hydrogen Bonding*; Oxford University Press: New York, NY, 1997.
2. Desiraju G. R., Steiner T. *The Weak Hydrogen Bond in Structural Chemistry and Biology*; Oxford University Press: New York, NY, 1999.
3. Grabowski S. J. *Hydrogen Bonding – New Insights*; Ed.; Springer: Dordrecht, Netherlands, 2006.
4 Scheiner S., Ed. *Molecular Interactions: From van der Waals to Strongly Bound Complexes*; Wiley: Chichester, UK, 1997.
5. Garcia-Viloca M., González-Lafont A., Lluch J. M. *J. Am. Chem. Soc.* 1997, *119*, 1081–1086.
6. Garcia-Viloca M., Gelabert R., González-Lafont A., Moreno M., Lluch J. M. *J. Phys. Chem. A* 1997, *101*, 8727–8733.
7. Perrin C. L., Nielson J. B. *Annu. Rev. Phys. Chem.* 1997, *48*, 511–544.
8. Mochida T., Izuoka A., Sugawara T., Moritomo Y., Tokura Y. *J. Am. Chem. Soc.* 1994, *101*, 7971–7974.
9. Malaspinna L. A., Edwards A. J., Woińska M., Jayatilaka D., Turner M. J., Price J. R., Herbst-Irmer R., Sugimoto K., Nishibori E., Grabowsky S. *Cryst. Grow. Des.* 2017, *17*, 3812–3825.
10. Hibbert F., Emsley J. *J. Adv. Phys. Org. Chem.* 1990, *26*, 255–379.
11. Emsley J. *Struct. Bond.* 1984, *57*, 147–191.
12. Gilli G., Bellucci F., Ferretti V., Bertolasi V. *J. Am. Chem. Soc.* 1989, *111*, 1023–1028.
13. Bertolasi V., Gilli P., Ferretti V., Gilli G. *Chem. Eur. J.* 1996, *2*, 925–934.
14. Mahmudov K. T., Pombeiro A. J. L. *Chem. Eur. J.* 2016, *22*, 16356–16398.
15. Brown R. S., Tse A., Nakashima T., Haddon R. C. *J. Am. Chem. Soc.* 1979, *101*, 3157–3162.
16. Demura Y., Kawato T., Kanatomi H., Murase I. *Bull. Chem. Soc. Jpn.* 1975, *48*, 2820–2824.
17. Svensson C., Abrahams S. C., Bernstein J. L., Haddon R. C., *J. Am. Chem. Soc.* 1979, *101*, 5759–5764.
18. Svensson C., Abrahams S. C. *Acta Crystallogr.* 1986, *B42*, 280–286.
19. Jackman L. M., Trewella J. C., Haddon R. C. *J. Am. Chem. Soc.* 1980, *102*, 2519–2525.
20. Rossetti R., Haddon R. C., Brus L. E. *J. Am. Chem. Soc.* 1980, *102*, 6913–6916.
21. Hameka H., de la Vega J. R. *J. Am. Chem. Soc.* 1984, *106*, 7703–7705.
22. Gilli P., Bertolasi V., Ferretti V., Gilli G. *J. Am. Chem. Soc.* 1994, *116*, 909–915.
23. Gilli G., Gilli P. *The Nature of Hydrogen Bond*; Oxford University Press: New York, NY, 2009.
24. Kovács A., Izvekov V., Zauer K., Ohta K. *J. Phys. Chem. A* 2001, *105*, 5000–5009.
25. Pal S. K., Itkis M. E., Reed R. W., Oakley R. T., Cordes A. W., Tham F. S., Siegrist T., Haddon R. C. *J. Am. Chem. Soc.* 2004, *126*, 1478–1484.
26. Pariyar A., Vijaykumar G., Bhunia M., Dey S. K., Singh S. K., Kurungot S., Mandal S. K. *J. Am. Chem. Soc.* 2015, *137*, 5955–5960.
27. Das A., Scherer T. M., Mondal P., Mobin S. M., Kaim W., Lahiri G. K. *Chem. Eur. J.* 2012, *18*, 14434–14443.
28. Dey S. K., Honecker A., Mitra P., Mandal S. K., Mukherjee A. *Eur. J. Inorg. Chem.* 2012, *35*, 5814–5824.
29. Mochida T., Torigoe R., Koinuma T., Asano C., Satou T., Koike K., Nikaido T. *Eur. J. Inorg. Chem.* 2006, *3*, 558–565.
30. Gu Y.-J., Yan B. *Inorg. Chim. Acta* 2013, *408*, 96–102.
31. Koelsch C. F., Anthes J. A. *J. Org. Chem.* 1941, *6*, 558–565.
32. Das A., Ghosh T. K., Dutta Chowdhury A., Mobin S. M., Lahiri G. K. *Polyhedron* 2013, *52*, 1130–1137.
33. Mandal S. K., Samanta S., Itkis M. E., Jensen D. W., Reed R. W., Oakley R. T., Tham F. S., Donnadieu B., Haddon R. C. *J. Am. Chem. Soc.* 2006, *128*, 1982–1994.
34. He G., Hou Y., Sui D., Wan X., Long G., Yun P., Yu A., Zhang M., Chen Y. *Tetrahedron* 2013, *69*, 6890–6896.
35. Bensch L., Gruber I., Janiak C., Müller T. J. J. *Chem. Eur. J.* 2017, *23*, 10551–10558.
36. Engdahl C., Gogoll A., Edlund U., *Magn. Reson. Chem.* 1991, *29*, 54–62.
37. Ozeki H., Takahashi M., Okuyama K., Kimura K. *J. Chem. Phys.* 1993, *99*, 56–66.
38. Kunze K. L., de la Vega J. R. *J. Am. Chem. Soc.* 1984, *106*, 6528–6533.
39. Svensson C., Abrahams S. C. *J. Appl. Crystallogr.* 1984, *17*, 459–463.
40. Dittrich B., Koritsanszky T., Luger P. *Angew. Chem. Int. Ed.* 2004, *43*, 2718–2721.
41. Dittrich B., Lübben J., Mebs S., Wagner A., Luger P., Flaig R. *Chem. Eur. J.* 2017, *23*, 4605–4614.
42. Dittrich B., Hübschle C. B., Pröpper K., Dietrich F., Stolper T., Holstein J. J. *Acta Crystallogr.* 2013, *B69*, 91–104.
43. Stewart R. F. *Acta Crystallogr.* 1976, *A32*, 565–574.
44. Hansen N., Coppens P. *Acta Crystallogr.* 1978, *A34*, 909–921.
45. Bensch L., Ebeling R., Arasu N. P., Schulze Lammers B., Mayer B., Müller T. J. J., Vázquez H. S., Karthäuser. submitted for publication.
46. Kabsch W. *Acta Crystallogr.* 2010, *D66*, 125–132.
47. Sheldrick G. M. *Acta Crystallogr.* 2015, *C71*, 3–8.
48. Krause L., Herbst-Irmer R., Sheldrick G. M., Stalke D. *J. Appl. Crystallogr.* 2015, *48*, 3–10.
49. Parsons S., Flack H. D., Wagner T. *Acta Crystallogr.* 2013, *B69*, 249–259.
50. Volkov A., Macchi P., Farrugia L. J., Gatti C., Mallinson P., Richter T., Koritsánszky T. XD2006. University at Buffalo USA, University of Milan, Italy, University of CNRIST Mand Middle Tennessee State University, NY Glasgow, UK Milan, Italy TN, USA, 2006.
51. Weininger D. *J. Chem. Inf. Comp. Sci.* 1988, *28*, 31–36.
52. Trucks G. W., Schlegel H. B., Scuseria G. E., Robb M. A., Cheeseman J. R., Scalmani G., Barone V., Mennucci B., Petersson G. A., Nakatsuji H., Caricato M., Li X., Hratchian H. P., Izmaylov A. F., Bloino J., Zheng G., Sonnenberg J. L., Hada M., Ehara M., Toyota K., Fukuda R., Hasegawa J., Ishida M., Nakajima T., Honda Y., Kitao O., Nakai H., Vreven T., Montgomery J. A. Jr., Peralta J. E., Ogliaro F., Bearpark M., Heyd J. J., Brothers E., Kudin K. N., Staroverov V. N., Kobayashi R., Normand J., Raghavachari K.,

Rendell A., Burant J. C., Iyengar S. S., Tomasi J., Cossi M., Rega N., Millam J. M., Klene M., Knox J. E., Cross J. B., Bakken V., Adamo C., Jaramillo J., Gomperts R., Stratmann R. E., Yazyev O., Austin A. J., Cammi R., Pomelli C., Ochterski J. W., Martin R. L., Morokuma K., Zakrzewski V. G., Voth G. A., Salvador P., Dannenberg J. J., Dapprich S., Daniels A. D., Farkas Ö., Foresman J. B., Ortiz J. V., Cioslowski J., Fox D. J., Frisch M. J. Gaussian 09 (Revision D.01). Gaussian, Inc.: Wallingford CT, 2013.

53. Jayatilaka D., Grimwood D. J. Tonto: A fortran based object-oriented system for quantum chemistry and crystallography. In *Computational Science – ICCS 2003. ICCS 2003. Lecture Notes in Computer Science*, vol 2660; Sloot P. M. A., Abramson D., Bogdanov A. V., Gorbachev Y. E., Dongarra J. J., Zomaya A. Y., Eds. Springer: Berlin, Heidelberg, 2003; pp. 142–151.
54. Hübschle C. B., Dittrich B. *J. Appl. Crystallogr.* 2011, *44*, 238–240.
55. Dittrich B., Hübschle C. B., Luger P., Spackman M. A. *Acta Crystallogr.* 2006, *D62*, 1325–1335.
56. Hübschle C. B., Dittrich B. *J. Appl. Crystallogr.* 2011, *44*, 238–240.
57. Svensson M., Humbel S., Froese R. D. J., Matsubara T., Sieber S., Morokuma K. *J. Phys. Chem.* 1996, *100*, 19357–19363.
58. Dittrich B., Pfitzenreuter S., Hübschle C. B. *Acta Crystallogr. A* 2012, *68*, 110–116.
59. Besler B. H., Merz K. M., Jr., Kollman P. A. *J. Comput. Chem* 1990, *11*, 431–439.
60. Rappe A. K., Casewit C. J., Colwell K. S., Goddard W. A., Skid W. M., Bernstein E. R. *J. Am. Chem. Soc.* 1992, *114*, 10024–10039.
61. Bannwarth C., Ehlert S., Grimme S. *J. Chem. Theory Comput.* 2019, *15*, 1652–1671.

Supplementary Material: The online version of this article offers supplementary material (https://doi.org/10.1515/zkri-2020-0022).